Wind and Structures, *Vol. 16, No. 5 (2013) 491-515*
DOI:http://dx.doi.org/10.12989/was.2013.16.5.491

Wind pressure characteristics for a double tower high-rise structure in a group of buildings

K.T. Tse*[1], D.Y. Wang[2] and Y. Zhou[2]

[1]*Department of Civil and Environmental Engineering, The Hong Kong University of Science and Technology, Hong Kong*
[2]*School of Civil Engineering, Guangzhou University, Guangdong, P.R. China*

(Received November 23, 2011, Revised June 21, 2012, Accepted June 21, 2012)

Abstract. Wind pressure characteristics on a double tower high-rise structure, which is disturbed by surrounding buildings, were investigated using large eddy simulation (LES) and 1:300 scale wind tunnel experiments. The computational simulation technique and wind tunnel experimental technique were described in detail initially. Comparisons of computational results with the experimental data have subsequently been carried out to validate the reliability of LES. Comparisons have been performed in detail for the mean and fluctuating pressure coefficients. Detailed explanations of each comparison were given in the paper. To study further on the pressure coefficients on the building surfaces, parametric studies on shape coefficient and spatial correlation were performed and investigated. The numerical and experimental results presented in this paper advance understanding on wind field around buildings and the application of LES and wind tunnel tests.

Keywords: computation; building; disturbance; pressure coefficient; spatial correlation; wind tunnel

1. Introduction

Simulation based on Computational Fluid Dynamics (CFD) has been a widely-used method of wind flow simulation around buildings for more than 20 years. Rapid development has been observed especially in recent studies. Traditional standard turbulence models, such as eddy viscosity-based models and various second-order stress models, are found to be inadequate in predicting unsteady flows around bluff bodies (Castro and Graham 1999, Cowan 1997, Lim *et al.* 2009, Leschziner 1993). Unsteady techniques such as discrete vortex methods and, particularly, large eddy simulation (LES) are found to be much more appropriate for simulating unsteady flow features (Murakami and Mochida 1995, Shah and Ferziger 1997, Murakami 1998, Fasel *et al.* 2002, Nozawa and Tamura 2002, Fureby 2007, Tominaga 2008). Rodi (1997) compared the performance of LES and Reynolds-averaged Navier-Stokes (RANS) calculations of vortex-shedding flow passing a square cylinder at Reynolds number, Re=22,000 and that of the 3D flow passing a surface-mounted cube at Re=40,000. The results showed that turbulence fluctuations were severely under-estimated by RANS, while LES was found more suitable and had

*Corresponding author, Assistant Professor, E-mail: timkttse@ust.hk

Copyright © 2013 Techno-Press, Ltd.
http://www.techno-press.org/?journal=was&subpage=8 ISSN: 1226-6116 (Print), 1598-6225 (Online)

great potential for complex flow calculations. The validity of LES in predicting flow around an obstacle under turbulent flow condition was also confirmed by Nozawa and Tamura (2002).

Breuer *et al.* (2003) investigated the variations of the predicted results among RANS, DES (detached-eddy simulation) and LES for the separated flow around a flat plate at high incidence.

The RANS computations were not able to capture the unsteady vortex shedding behaviour and both two- and three-dimensional RANS predictions led to the same steady-state results. The asymmetric vortex shedding motion was well reproduced by DES and LES. However, the free shear layer originating from the leading edge of the plate was not well reproduced by DES. Kose and Dick (2010) presented a numerical study of the flow around a cubical building by RANS, hybrid RANS/LES and LES at $Re=4\times10^6$. The results obtained by LES were the most accurate for coarse grid simulations. A detailed comparison between LES and experiment of both the inflow boundary layer and the flow field around a cube was performed by Lim *et al.* (2009). The results confirmed that LES is a viable tool for use in wind engineering problems concerning flow over isolated bodies.

It is well-known that there is rarely a case where only one single high-rise building is built in a city district. Many more regional groups of high-rise buildings are built in major cities, which induce more complicated structural wind characteristics because of interaction and obstruction effects among buildings. Moreover, existing study results on wind characteristics of flow around single building and also some design parameters stipulated in international design codes, may not be applicable to buildings under such wind condition. Therefore the structural wind characteristics influenced by surrounding buildings have been a subject of interest to researchers and engineers in view of its significance for the evaluation of building designs. Zhou (2011) studied wind characteristics around a tall structure, which is disturbed by surrounding buildings, using experimental and numerical methods. The results showed that pressure coefficients were greatly disturbed by surrounding proximity. Cheng *et al.* (2003) discussed the predictive performance of LES with various dynamic sub-grid scale models for a fully developed turbulent flow around a matrix of cubes. Su and Chen (2006) predicted the wind-induced surface pressures and wind environment around a complex-shaped high-rise building with annex using the standard k-ε model and the RNG k-ε model. Ma *et al*. (2007) investigated the wind environment around a single building and a building complex based on the Reynolds averaged N-S equations and the RNG k-ε turbulence model. Wang *et al*. (2003) predicted wind-induced pressures on a low-rise single house with gable roofs and a building complex consisting of six low-rise houses with gable roofs using numerical simulation.

This paper aims to assess the wind pressure characteristics of a double tower high-rise structure under the interaction and obstruction effects of surrounding buildings. The study results will assist engineers and researchers to acquire a better understanding of the potential risks involved, such as extreme pressure and unfavorable wind direction, when designing a similar double tower. To achieve this, the present paper contains CFD and wind tunnel test results using a 1:300-scale pressure model. The CFD simulations were performed using the LES method. Comparisons between LES predictions and measured wind tunnel data were made in terms of the mean pressure coefficients for a number of pressure taps around the outer and inner surfaces of the double tower building. Comparisons were also carried out for disturbance effect and spatial correlation of the fluctuating pressure and interaction and obstruction effect. In addition, the reliability of LES method in simulating flow around a group of buildings was also revealed. CFD analyses were conducted to investigate the capability and accuracy of the LES method in simulating the wind

flow in a group of building complex. The details of the CFD simulations and wind tunnel pressure tests are outlined as follows.

2. Computational simulation technique

2.1 Governing equations

LES is a well-known mathematical model for turbulence used in computational fluid dynamics and the governing equations are briefly summarized below for ease of reference. Smagorinsky (1963) proposed the LES method in order to simulate atmospheric air currents, and many of the issues unique to LES were first explored by Deardorff (1970). LES is currently applied in a wide variety of engineering applications, including combustion (Pitsch 2006), acoustics (Wagner *et al.* 2007), and simulations of the atmospheric boundary layer (Stoll and Porté-Agel 2008, Sarkar and Sarkar 2009).

A box filter was applied as a filter kernel and incompressible flow was assumed in the present study. For incompressible flow, the continuity equation and Navier-Stokes equation are filtered, yielding the filtered incompressible continuity equation and the filtered Navier-Stokes equation

$$\begin{cases} \dfrac{\partial \overline{u}_i}{\partial x_i} = 0 \\ \dfrac{\partial \overline{u}_i}{\partial t} + \dfrac{\partial}{\partial x_j}\left(\overline{u_i u_j}\right) = -\dfrac{1}{\rho}\dfrac{\partial \overline{p}}{\partial x_i} + \nu \dfrac{\partial}{\partial x_j}\left(\dfrac{\partial \overline{u}_i}{\partial x_j} + \dfrac{\partial \overline{u}_j}{\partial x_i}\right) = -\dfrac{1}{\rho}\dfrac{\partial \overline{p}}{\partial x_i} + 2\nu \dfrac{\partial}{\partial x_j}\overline{S}_{ij} \end{cases} \tag{1}$$

where $\overline{S}_{ij}$ is the rate-of-strain tensor, $\overline{p}$ is the filtered pressure field, $\overline{u_i u_j}$ is the filtered advection term, which is the chief cause of difficulty in LES simulation. The filtered advection term $\overline{u_i u_j}$ can be split up as follows (Leonard 1974)

$$\overline{u_i u_j} = \tau_{ij}^r + \overline{u}_i \overline{u}_j \tag{2}$$

where τ_{ij}^r is the residual stress tensor. From Eqs. (1) and (2), the filtered Navier-Stokes equation become

$$\frac{\partial \overline{u}_i}{\partial t} + \frac{\partial}{\partial x_j}\left(\overline{u}_i \overline{u}_j\right) = -\frac{1}{\rho}\frac{\partial \overline{p}}{\partial x_i} + 2\nu \frac{\partial}{\partial x_j}\overline{S}_{ij} - \frac{\partial \tau_{ij}^r}{\partial x_j} \tag{3}$$

The residual stress tensor τ_{ij}^r was decomposed by Leonard (1974) as

$$\tau_{ij}^r = L_{ij} + C_{ij} + R_{ij} \tag{4}$$

where R_{ij} is the Reynolds stress-like term representing interactions among the sub-grid scales

(SGS), C_{ij} is the Clark tensor (Clark 1979) representing cross-scale interactions between large and small scales, and L_{ij} is the Leonard tensor representing interactions among large scales. One of the most important and challenging work in LES simulation is to calculate the unclosed term τ_{ij}^r.

Based on Boussinesq's assumption, a well-known model was developed by Smagorinsky (1963) and used in the first LES simulation by Deardorff (1970). The rate-of-strain tensor $\overline{S}_{ij}$ was defined as

$$\tau_{ij}^r = \tau_{ij} - \frac{\tau_{kk}\delta_{ij}}{3} = -2\nu_t \overline{S}_{ij} \tag{5}$$

where δ_{ij} is the Kronecker delta, ν_t is the eddy viscosity, τ_{kk} is sub-grid scale turbulence kinetic energy, and τ_{ij} is the sub-grid scale Reynolds stress. The new pressure P can be obtained by adding τ_{kk} into the filtered pressure

$$P = \overline{p} + \frac{\tau_{kk}}{3} \tag{6}$$

It is evident that ν_t can be expressed as a function of the rate-of-strain tensor $\overline{S}_{ij}$ and the sub-grid length L_s

$$\nu_t = (L_s)^2 \left|\overline{S}_{ij}\right| = (L_s)^2 \sqrt{2\overline{S}_{ij}\overline{S}_{ij}} \tag{7}$$

The sub-grid length L_s is proportional to the filter width Δ

$$L_s = C_s \Delta = C_s \left(\Delta_x \Delta_y \Delta_z\right)^{1/3} \tag{8}$$

where Δ_x, Δ_y and Δ_z are grid scales in x, y and z directions, respectively. C_s is Smagorinsky constant. In general, C_s can be taken as approximately 0.16 for isotropic turbulence. However, smaller values are usually applied in LES simulation in order to improve the precision of computational results (Breuer 2003). In the present work, the Smagorinsky constant C_s in all computational cases was taken as 0.1. Even though dynamic model is superior, it was not considered in this study. The reason for that lies in the SGS type of model within the LES mode of the DES formulation. The way the modified S-A model is used as an SGS model in the LES mode strongly resembles the Smagorinsky model with a corresponding constant C_{DES} (Breuer 2003).

2.2 Computational model

In this study, to compare the results of LES with the experimental data presented in the next section, a 1:300 scaled numerical model of 0.16 m × 0.14 m × 0.75 m (i.e., $L \times B \times H$) was

designed. In order to eliminate flow obstacle effect on the inflow and outflow boundary conditions (Murakami 1998), the length of inflow, outflow and side-flow of the computational domain are 5*H*, 12*H* and 5*H*, respectively, as shown in Fig. 1. The total height of the computational domain is 3*H* in order to keep the blockage ratio less than 3% as discussed by Murakami (1998). The Reynolds number based on the width *L* and inflow velocity *U(z)* at *z=H* is about 5.4×10^5. Both structured and unstructured grids were used for mesh generation, as shown in Fig. 1. For zones near the bluff body, an unstructured mesh was generated while for zones outside the unstructured mesh, the structured mesh was applied. One important advantage of this arrangement is that it is convenient to generate a mesh fine enough in the neighborhood of the building surfaces while keeping the mesh in far-field zones from the building surfaces unchanged or in a proper coarser mesh. The ADINA (2005) platform, which has the capacity of manage both structured and unstructured grids in its solver, was adopted in this study. The average distance of the first layer of nodes from the surface is about *L*/5000 in X direction and *B*/5000 in Y direction with same growth factor of 1.2, which are smaller than the values suggested by Murakami (1998) (i.e., *D*/1000) and Huang (2006) (i.e., *D*/4000), so as to ensure that the wall unit $y^+<5$ is satisfied. The maximum grid size used in the far-field from the building is about *H*. No-slip boundary conditions were imposed on the velocity near the solid boundaries. The Reichardt wall-law was then used to derive the shear stresses caused by the presence of the wall (Hinze 1959, Camarri *et al.* 2002). This wall-law has the advantage of describing the velocity profile, not only in the laminar sub-layer ($y^+<5$), but also in the logarithmic region of a turbulent boundary layer ($y^+\geqq40$) and in the intermediate region.

This guarantees correct asymptotic behavior at the wall of the SGS terms in the Smagorinsky model. In total, over 800,000 3D grid elements were generated in the present simulation. As the grid size around the target and surrounding building is very small, the number of unstructured 3D grid elements around the buildings is about 300,000. However, the grid size of far-field from the buildings is relatively coarse so as to reduce the computing time. Computations were carried out on 16 Xeon E5580 3.2 GHz CPUs and requires about 16GB of Infineon memory and about 8 days of CPU time for the whole simulation. The numerical time step for the transient simulation was 5×10^{-4} sec and 8000 steps, which is equivalent to 4 seconds, are needed to collect data for computational stability purposes. The statistical average of flow field was taken for the last 4000 steps, equivalent to 2 sec.

2.3 Boundary conditions

It is well known that boundary conditions of the computational domain and bluff bodies should be modeled close enough to those employed in experiments, especially for the inflow boundary, in order to obtain better agreement between numerical and experimental results. At the same time, reasonable boundary conditions will also be helpful of saving computational time. For the inflow boundary condition, both the mean and fluctuating wind velocity were considered. The mean wind velocity can be achieved by matching a log-law profile with a typical shear exponent of the real conditions (Obasaju 1992)

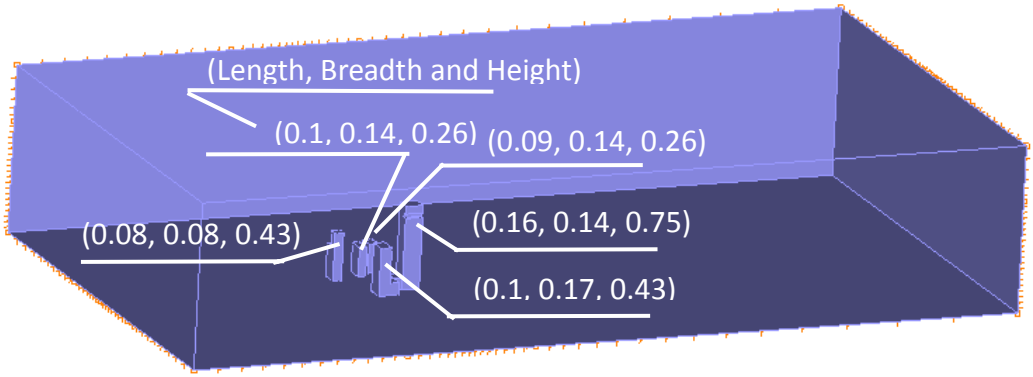

(a) Computational domain (Unit: m)

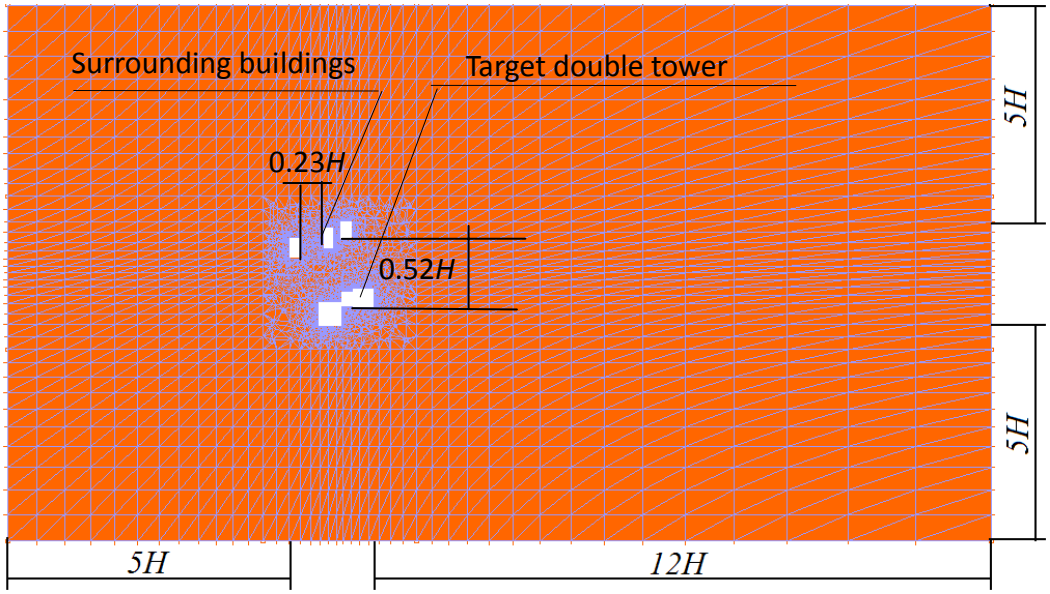

(b) Grid distribution

Fig. 1 A 1:300 scaled numerical model: (a) computational domain and (b) grid distribution

$$\begin{cases} v(z) = 2.5v^* \log_e(40)\left(\dfrac{z}{40Z_0 + D}\right)^{0.25} & \left(\dfrac{z-D}{Z_0}\right) < 40 \\ v(z) = 2.5v^* \log_e\left(\dfrac{z-D}{Z_0}\right) & 40 \le \left(\dfrac{z-D}{Z_0}\right) \le 1000 \end{cases} \tag{9}$$

where, $v(z)$ is the horizontal wind speed at elevation z, v^* is the surface friction velocity defined as $(\tau_\circ / \rho)^{0.5}$ with $\tau_\circ$ being the surface shear stress, D is the height of the zero plane above ground, Z_0 is the surface roughness length parameter. The height of the gradient wind is 450 m.

Based on the procedure suggested by Kraichnan (1970) for generation of an isotropic continuous flow field satisfying a spectrum of Dirac function, a new general inflow turbulence generation method for large eddy simulation, also called the discretizing and synthesizing random flow field generation (DSRFG) technique, was proposed by Huang *et al.* (2010) and Li *et al.* (2007). The isotropic fluctuating velocity in **X** space was synthesized by the following superposition of harmonic functions (Huang *et al.* 2010)

$$u_i(\mathbf{X},t) = \sum_{n=1}^{N}\left[p_i^n \cos\left(k_j^n x_j + \omega_n t\right) + q_i^n \sin\left(k_j^n x_j + \omega_n t\right)\right] \tag{10}$$

$$p_i^n = \varepsilon_{ijm}\varsigma_j^n k_m^n, \quad q_i^n = \varepsilon_{ijm}\xi_j^n k_m^n, \quad \varsigma_j^n, \xi_j^n, \omega_n \in N(0,1), \quad k_j^n \in N(0,1/2)$$

where k and ε are the turbulence kinetic energy and the turbulence dissipation rate, respectively, ε_{ijm} is the permutation tensor used in vector product operation, k_j^n and ω_n, respectively, represent a sample of n wave-number vectors and frequencies of the modeled turbulence spectrum. Detailed information about Eq. (10) was given by Huang *et al.* (2010). The first advantage of the DSRFG is that continuity condition, $div(\mathbf{u}) = 0$, can be strictly ensured.

Secondly, the fluctuating velocity generated in the inflow condition satisfies a specified power spectrum density function and the spatial correlation of inflow condition can be adjusted by using different scaling factors.

At the outflow, convective boundary condition is applied for velocity and pressure using Eq. (11).

$$\partial/\partial t + c\left(\partial/\partial x\right) = 0 \tag{11}$$

where c is taken to be the bulk velocity so as to ensure global mass conservation. Slip conditions were assumed for velocity on the 2 sides and top surfaces of the computation domain. With this kind of boundary condition, one has $\partial U/\partial y = \partial U/\partial w = V = W = 0$. A no-slip condition was used for velocity on the ground surface, u_n = 0. The Neumann condition for pressure was employed on building surfaces and the computation domain, as the pressure gradient orthogonal to the surfaces is equal to zero.

3. Experimental technique

The experiments were carried out in a large wind tunnel at Guangdong Provincial Academy of Building Research. The wind tunnel has a measurement section of 10 m (length)×3 m (width) ×2 m (height), with a maximum wind velocity of 20 m/s. More details of the wind tunnel and its

functional characteristics can be found in reference GPABR.

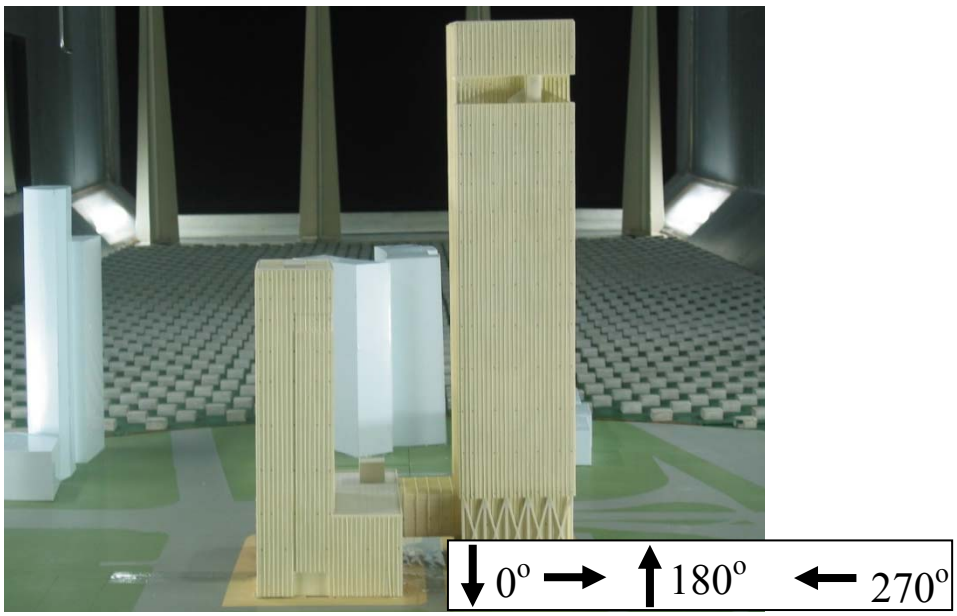

Fig. 2 Wind tunnel pressure test model of double tower high-rise structure

A 1:300 scale rigid model of the double tower, as shown in Fig. 2, was constructed and tested to measure building surface pressure. In order to capture accurately the most unfavorable distribution of wind pressure on building surfaces, basic principle, such as uniform rule along structural height, was adopted to arrange pressure taps. Besides, encryptions plan of arranging pressure taps at some areas of unfavorable wind load, such as structural corners, was also adopted. The model was installed with 26 layers of pressure taps over the double tower, resulting in a total of 382 pressure taps on the building surfaces. Fig. 3 shows the elevations of the 26 layers of pressure taps and the corresponding coding of each layer while Fig. 4 shows specific locations of the pressure tap distribution at different height. It is worth mentioning that the pressure taps at height of parapet, that is the height of 210.7 m and 125.2 m for the main and sub-main towers, respectively, are arranged on surfaces of both sides of parapet. The coding of the pressure taps on the inside surfaces of the parapet are DAP and DBI for the main and sub-main towers, respectively. The primary aim is to understand pressure and suction forces imposed on the parapet and their influence on the wind field, which is essential and important for a proper design of parapet.

A boundary-layer wind tunnel test corresponding to an open terrain (i.e., Type B) in the Chinese code (2002), was simulated at GPABR wind tunnel. The fluctuating wind velocity was measured at various heights at the center of the working section using a hot-wire anemometer. Measured and target gust wind speed profiles were normalized with respect to the value at building height and are presented in Fig. 5(a), together with the measured and target turbulence intensity profiles. The wind tunnel results are reasonably consistent with the targeted profiles, with the difference generally not exceeding 1%. It can also be seen from Fig. 5(b) that the corresponding

spectrum of longitudinal wind speed at building height is comparable to a Harris-von Karman spectrum with a longitudinal turbulence length scale of approximately 190 m at prototype scale. The experimental velocity at 750 mm height in the wind tunnel, corresponding to the height of 225.6 m of the actual structure, was 8.3 m/s. The sampling frequency was taken at 313 Hz. The wind tunnel experiments were performed for 24 wind directions. The free stream flow conditions were:

- velocity at the top of the double tower model: U=8.3 m/s;
- pressure: P=1.01×105 Pa;
- temperature: T=20°C;
- air density: ρ=1.2 kg/m^3;
- kinematic viscosity: v=0.000015 m^2/s; and
- wind direction: 0°~360° with an interval of 15°, as shown in Fig. 4.

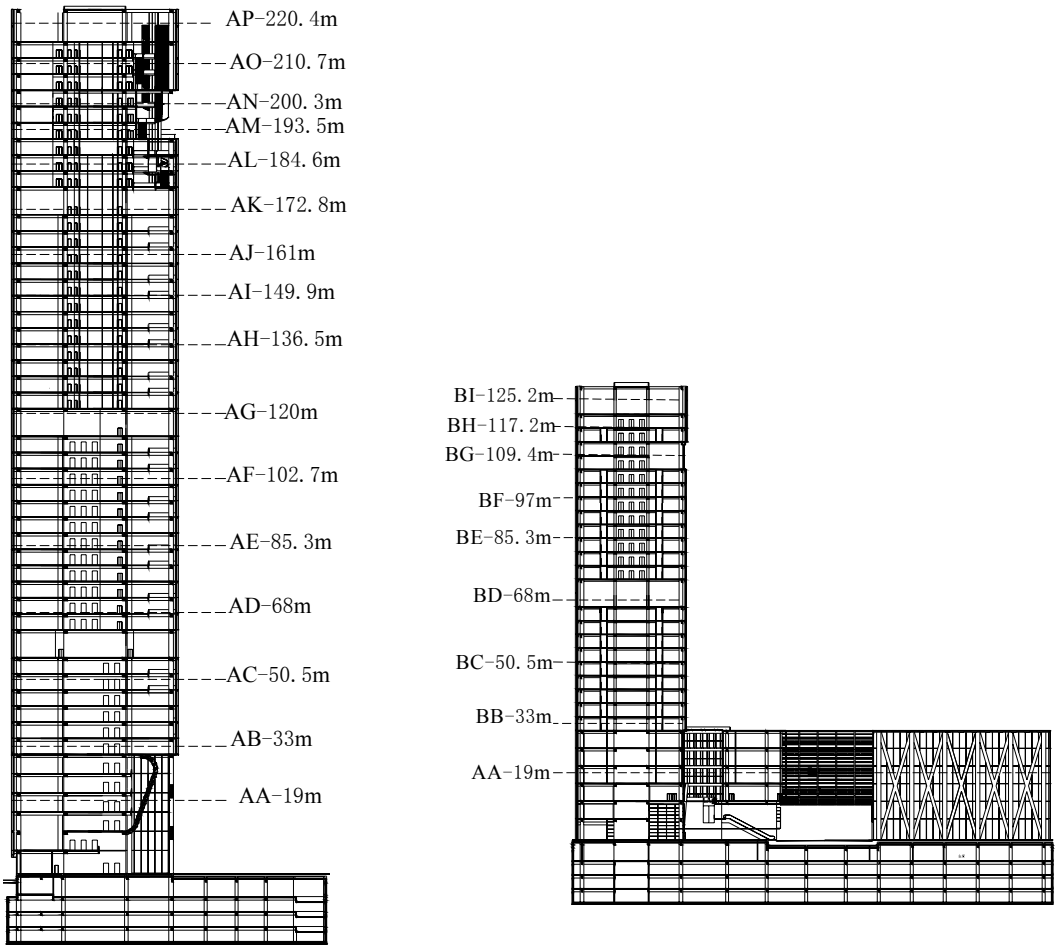

(a) Main tower (b) Sub-main tower

Fig. 3 Distribution of pressure taps along the building heights

Each pressure tap is connected to the Hyscan System 2000 using both ZOC 23 and ZOC 33 scanners with 10 in H_20 range, using a single tubing without any restrictor. The amplitude and phase distortion due to the tubing system were compensated by numerical post-processing. A white noise signal source was employed to calibrate the dynamic characteristics of each plastic tube. The dynamic distortion resulting from the tubing response was corrected based on the resulting transfer function. The pressure signal correction was performed by dividing the real and the imaginary parts of the Fast Fourier Transform (FFT) pressure signal with the real and imaginary parts of the transfer function of each pressure tube. The signal was then inversely-transformed to produce the corrected pressure time history (Mahmoud *et al.* 2008).

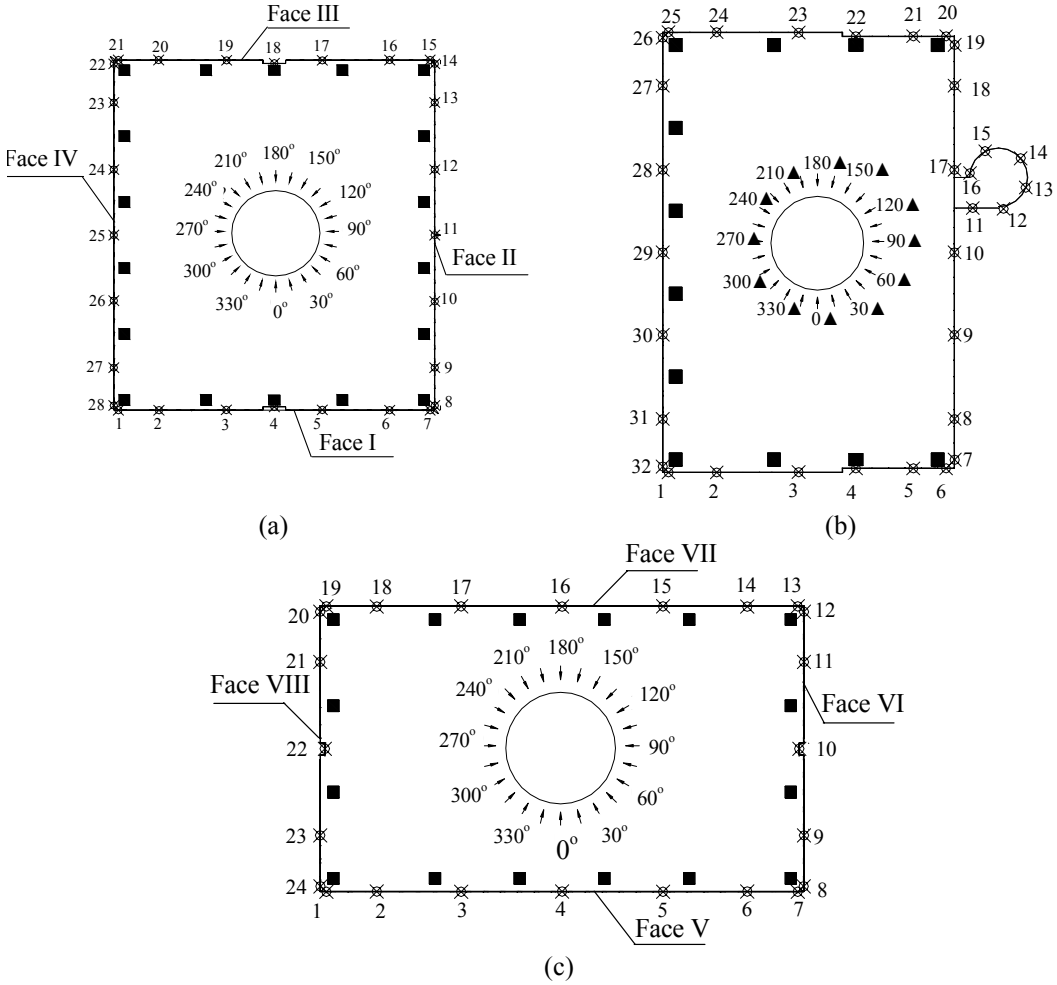

Fig. 4 Location of the pressure tap distribution on (a) Level AB~AL, AO, AP, DAP, (b) Level AM, AN, and (c) BB~BI, DBI

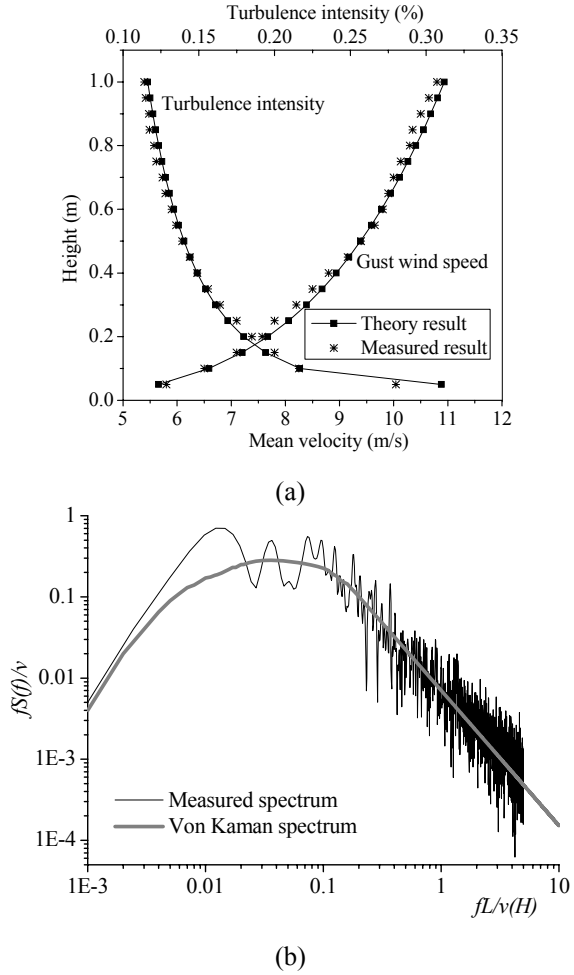

Fig. 5 Wind characteristics and longitudinal wind spectrum (a) wind characteristics and (b) longitudinal wind spectrum

4. Data processing

Pressure data obtained from both computational simulation and experimental technique is processed using equations as shown in Table 1. External pressures were normalized with respect to the mean wind pressure at height of *H*. Instantaneous pressure coefficients were determined at each pressure tap location and subsequently analyzed to determine maximum, minimum, mean, and standard deviation of pressure coefficients. A shape coefficient, which is defined as the ratio between the actual pressure of building surface induced by wind action and the velocity pressure of inflow wind, is used to account for the influences of the shape and size of a building. A weighted average shape coefficient describes the distribution of static pressure on a building surface under wind action. The spatial correlation of fluctuating wind represents pressure dependency of two pressure taps - an important indication of the flow pattern spatially and the

corresponding transmission pattern.

Table 1 Data processing equations

Wind pressure coefficient	$C_{pi}(n)=\dfrac{p_i(n)}{\rho \mathrm{U}_{ref}^2/2} \quad (n=1\mathrm{L}\ N)$
Mean wind pressure coefficient	$\overline{C}_{pi}=\sum_{n=1}^{N}\dfrac{C_{pi}(n)}{N}$
Fluctuating wind pressure coefficient	$C_{pi,rms}=\sqrt{\sum_{n=1}^{N}\dfrac{\left(C_{pi}(n)-\overline{C}_{pi}\right)^2}{N-1}}$
Shape coefficient	$\mu_{si}=\dfrac{\overline{C}_{pi}\mu_{zr}}{\mu_{zi}}$
Weighted average shape coefficient	$\mu_s=\dfrac{\sum_i \mu_{si}A_i}{A}$
Correlation coefficient of fluctuating pressure	$\rho_{ij}=\dfrac{E\left[\left(C_{pi}(n)-\overline{C}_{pi}\right)\left(C_{pj}(n)-\overline{C}_{pj}\right)\right]}{C_{pi,rms}C_{pj,rms}}$

As shown in Table 1, i is the number of pressure tap; N is the sample length of the wind pressure time series, N =4096; ρ=1.2kg/m^3 is air density; U_{ref} is wind velocity at height of H; z_i is the height of the i^{th} pressure taps; μ_{zr} is wind pressure coefficient at reference height; μ_{zi} is wind pressure coefficient of the i^{th} pressure taps; μ_{si} is the shape coefficient of the i^{th} pressure taps; A_i is the tributary area of the i^{th} pressure taps; A is the total surface area.

5. Results and discussion

5.1 Mean pressure coefficient

Based on the formulae given in Table 1, the mean pressure coefficients of the double tower were determined from the wind tunnel pressure measurements for 24 wind incident directions and subsequently compared with the numerical simulations. Tables 2 and 3 show the maximum and minimum mean pressure coefficients of the main and sub-main towers obtained from wind tunnel tests. Results show that the most unfavorable wind direction was 90º, at which winds are normal to the building surface. In this wind direction, both main and sub-main towers were imposed by the maximum positive mean wind pressure on the windward faces as no building exists in the upwind direction. And the maximum negative wind pressures occurred on the side surfaces. For the opposite direction at 270º, the maximum mean pressure coefficients decrease as there are

surrounding buildings located in the upwind direction and the double tower building falls inside the wake of the buildings. The decrease in the maximum positive mean pressure coefficients in a certain extent was attributable to the shielding effects of the upstream buildings, which is in good agreement with the results of Gu and Huang (2003). For 0º and 180º wind incident directions, although there is no building in the upwind direction, interaction and obstruction effect between the main and sub-main towers exists. In this case, the mean pressure coefficients were slightly reduced.

Table 2 Maximum and minimum mean pressure coefficients of the main tower

Direction	0º	15º	30º	45º	60º	75º	90º	105º	120º	135º	150º	165º
MIN	-1.5	-1.27	-1.08	-1.12	-1.12	-1.54	-1.77	-1.75	-1.12	-0.99	-0.88	-1.23
Taps	AF28	AO8	AN13	AO14	AN20	AL7	AO7	AL15	AB7	AB7	AF1	AO14
MAX	0.91	0.94	0.99	0.91	0.92	0.92	0.98	0.96	0.92	0.94	0.92	0.89
Taps	AN4	AN4	AO6	AN7	AN7	AN12	AN10	AN13	AN18	AN16	AN20	AN21
Direction	180º	195º	210º	225º	240º	255º	270º	285º	300º	315º	330º	345º
MIN	-1.36	-1.34	-1.16	-1.06	-1.04	-1.3	-1.2	-1.3	-0.7	-0.75	-0.98	-1.15
Taps	AO14	AO13	AO13	AF28	AF28	AP21	AD21	AP1	AC7	AL7	AO9	AP28
MAX	0.94	0.92	0.88	0.85	0.94	0.9	0.96	0.96	0.93	0.91	0.93	0.87
Taps	AN22	AN23	AN24	AM25	AN27	AM28	AN29	AN30	AO27	AO28	AN2	AN2

Table 3 Maximum and minimum mean pressure coefficients of the sub-main tower

Direction	0º	15º	30º	45º	60º	75º	90º	105º	120º	135º	150º	165º
MIN	-1.16	-1.09	-0.92	-1.05	-1.18	-1.03	-1.36	-0.93	-0.92	-0.95	-0.96	-1.33
Taps	BI24	BI8	BE8	BH12	BG12	BI13	BI7	BE8	BE8	BE8	BE8	BI12
MAX	0.72	0.79	0.77	0.75	0.81	0.73	0.80	0.78	0.76	0.77	0.74	0.74
Taps	BF4	BF5	BF5	BH7	BH8	BG10	BG10	BH11	BH12	BG13	BH14	BH14
Direction	180º	195º	210º	225º	240º	255º	270º	285º	300º	315º	330º	345º
MIN	-1.34	-0.96	-0.94	-0.96	-0.93	-0.9	-0.92	-1.03	-1.23	-1.2	-0.99	-1.06
Taps	BI12	BE8	BE8	BE8	BE8	-0.9021	BE8	BI1	BI19	BG20	BG20	BI24
MAX	0.64	0.08	0.58	0.76	0.71	0.76	0.39	0.56	0.48	0.58	0.75	0.75
Taps	BH14	BD21	BD20	BH20	BH20	BG21	BB19	BH22	BG23	BG1	BF1	BF3

It can be seen that almost all maximum negative pressure coefficients were found at the pressure taps around the building corners, e.g., pressure taps AO14, AB7, AF28 and AL7 for 45°, 135°, 225° and 315°, respectively. This is, in general, caused by the flow separation at the corners, where strong vortex shedding takes place. The maximum positive mean pressure coefficients occurred on the centerline of the front face at a height of about 0.8*H*-0.9*H*. For example, the maximum positive mean pressure occurred at tap AN22 at a height of 0.87*H,* for a wind incident direction of 180º. Similar results were found for other wind directions.

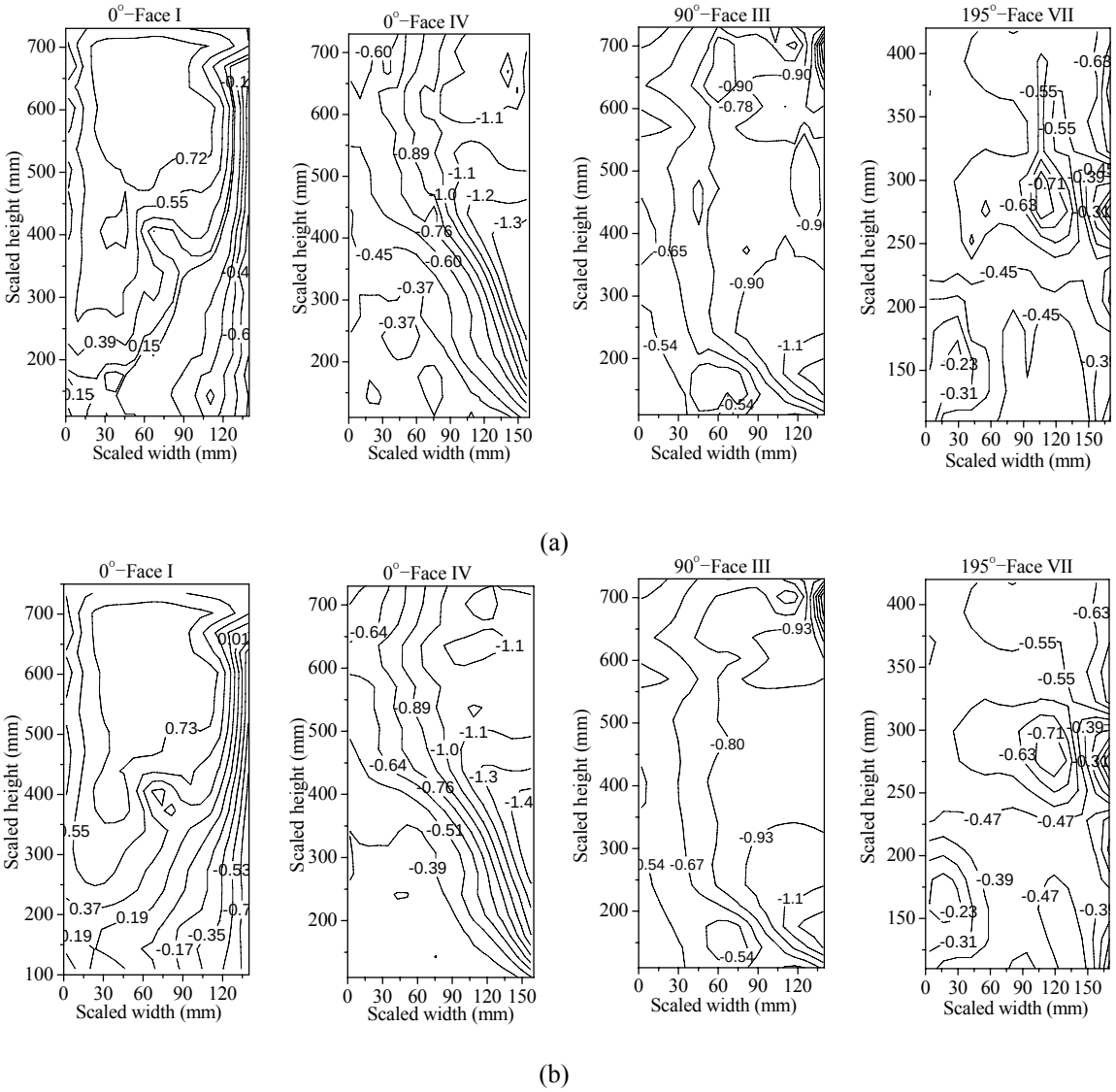

Fig. 6 Mean pressure coefficient contours: (a) numerical simulation and (b) experimental measurements

Mean pressure coefficient contours obtained from numerical simulations and experimental results are shown in Fig. 6. It can be seen from the figure that although there were some discrepancies noted on the higher level and the rear face, the mean pressure distributions of the numerical results generally are in good agreement with the experimental results. The small discrepancies were possibly caused by the dissimilarities between the numerical and experimental studies in dealing with model boundary conditions, turbulence intensity, blocking effects etc.

It is well-known that the mean pressure coefficients on the windward face are largely positive for an isolated building (Huang *et al*. 2006, Gomes *et al*. 2005). However, in this study the mean pressure coefficients were greatly affected by the interaction and obstruction effects between the main and sub-main towers and the upstream buildings. For example, the mean pressure coefficients of the main tower on the front face were negative on the lower level for 0º wind incident direction, attributed to the influence of the sub-main tower, as shown in Fig. 6. The mean pressure on the side and back faces were also greatly disturbed, as discussed in detail in the following sections.

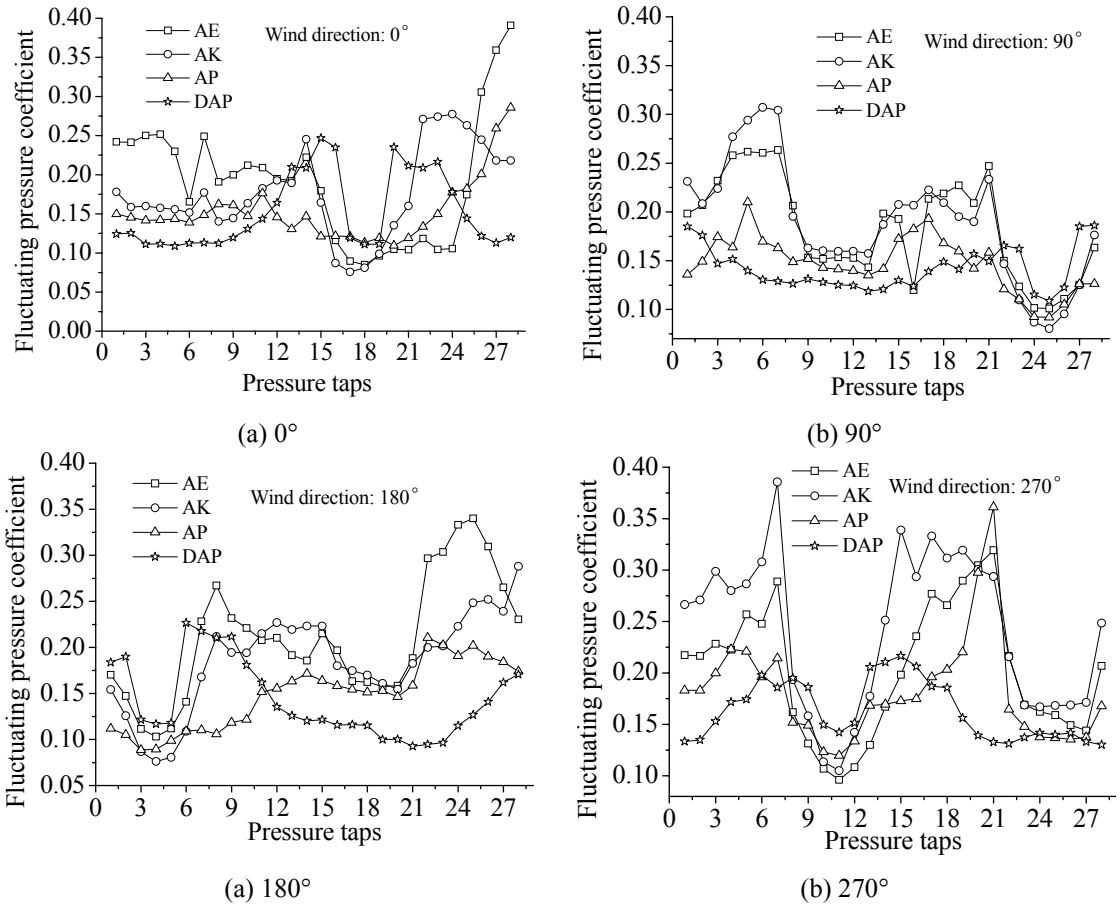

(a) 0° (b) 90°

(a) 180° (b) 270°

Fig. 7 Fluctuating pressure coefficients in different wind direction obtained from LES

5.2 Fluctuating pressure coefficient

A comparison of the fluctuating pressure coefficients obtained from numerical simulation and experimental results is shown in Table 4 and Fig. 7. Fluctuating pressure coefficients of different taps on the front faces are largely of similar values, as shown in Fig. 7, which means that flow on the front faces is relatively stable. At the corner, the fluctuating pressure coefficients increase as stronger vortex motion is generated. On the side faces, larger fluctuating pressure coefficients relative to those on the front faces can be observed, especially for the region at the corner, due to the flow separation. The reason is that strong and coherent vortex motion appears on the side faces which produces the increase of the fluctuating pressure. On the back faces, the variation of the fluctuating pressure coefficients are relatively more complicated, attributed to the irregular and disorder vortices generated in the wake flow. It can also be noticed that the pressure coefficients on the lower parts of the experimental model are relatively larger than those on the upper parts, as interaction and obstruction effects exist on the lower part, between the main and sub-main towers. Furthermore, it can also be found that the fluctuating pressure coefficients on inner surfaces of the parapet are smaller than the outer surfaces.

A certain deviation can be observed for the fluctuating pressures at the building corners between experiment and simulation. One of the reasons is that flow separations occur and a series of vortex sheds on the two sides of the building and the wake region, for which it is challenging to simulate accurately using the numerical method. However, the discrepancy of the fluctuating pressure coefficients between experiment and computational simulation is by and large insignificant, with errors less than 5%. This is comparable to typical repeatability in wind tunnel data.

5.3 Interaction and obstruction effect

To study the interaction and obstruction effect among buildings, an interaction and obstruction factor γ is defined as

$$\gamma=\mu_s/\mu_{sn} \tag{12}$$

where μ_s is the shape coefficient with the interaction and obstruction effect, μ_{sn} is the shape coefficient without the interaction and obstruction effect.

The variation of the interaction and obstruction factor along the height of both the main and sub-main towers in different wind directions is shown in Fig. 8. A noticeable discrepancy can be found between experimental and numerical results, especially for areas of negative wind pressure, such as the side and back faces. The reason of such a phenomenon may be that boundary conditions were not the same as those of wind tunnel tests, and the turbulence model could not capture accurately the vortex motion. However, in general, good agreement between results of the two techniques is found, and the discrepancy is acceptable from an engineering point of view. Therefore simulation with LES method is feasible for prediction of the flow field around the double tower buildings.

Table 4 Comparison of fluctuating pressure coefficients between numerical simulation and experimental results

Wind direction			Front face						Side face						Back face			
0°	Pressure taps		1	2	4	6	7	8	9	11	13	14	15	16	18	20	21	
	AE	Exp.	0.242	0.241	0.252	0.165	0.249	0.191	0.200	0.209	0.193	0.222	0.179	0.059	0.085	0.105	0.104	
		Num.	0.261	0.245	0.259	0.170	0.268	0.201	0.201	0.210	0.181	0.220	0.185	0.056	0.090	0.111	0.113	
		Err.	7.82%	1.45%	2.84%	2.81%	7.59%	5.36%	0.58%	0.31%	6.04%	1.07%	3.33%	4.97%	5.88%	5.99%	8.96%	
	AH	Exp.	0.189	0.153	0.147	0.131	0.199	0.190	0.196	0.230	0.230	0.278	0.224	0.111	0.081	0.110	0.123	
		Num.	0.184	0.147	0.144	0.134	0.217	0.211	0.216	0.223	0.223	0.295	0.240	0.113	0.078	0.105	0.123	
		Err.	2.26%	3.54%	2.65%	2.48%	8.72%	11.06%	10.15%	3.13%	3.16%	6.03%	6.97%	1.78%	3.27%	4.34%	0.70%	
90°	Pressure taps		8	9	11	13	14	15	16	18	20	21	22	23	25	27	28	
	AC	Exp.	0.177	0.154	0.148	0.147	0.223	0.272	0.286	0.199	0.197	0.240	0.144	0.133	0.115	0.176	0.185	
		Num.	0.175	0.157	0.144	0.153	0.227	0.302	0.303	0.212	0.206	0.259	0.146	0.126	0.116	0.183	0.201	
		Err.	1.04%	2.03%	2.68%	4.55%	1.85%	11.00%	6.20%	6.28%	4.63%	7.73%	1.08%	5.15%	0.36%	3.75%	8.91%	
	AI	Exp.	0.201	0.151	0.152	0.142	0.171	0.174	0.178	0.198	0.210	0.260	0.144	0.120	0.083	0.135	0.204	
		Num.	0.212	0.150	0.155	0.147	0.180	0.190	0.169	0.194	0.214	0.273	0.150	0.114	0.078	0.141	0.214	
		Err.	5.69%	0.58%	1.56%	3.56%	5.61%	9.27%	5.08%	2.09%	1.61%	5.19%	3.99%	4.74%	5.84%	4.36%	4.79%	
270°	Pressure taps		22	23	25	27	28	1	2	4	6	7	8	9	11	13	14	
	AL	Exp.	0.126	0.116	0.236	0.358	0.383	0.220	0.204	0.192	0.135	0.270	0.251	0.255	0.264	0.239	0.258	
		Num.	0.135	0.119	0.242	0.349	0.414	0.206	0.191	0.196	0.132	0.255	0.279	0.269	0.268	0.222	0.257	
		Err.	6.52%	2.93%	2.24%	2.56%	8.20%	6.46%	6.37%	2.22%	2.47%	5.55%	11.14%	5.64%	1.66%	7.02%	0.26%	
	AO	Exp.	0.209	0.220	0.246	0.231	0.233	0.175	0.168	0.164	0.150	0.175	0.286	0.259	0.222	0.178	0.155	
		Num.	0.227	0.215	0.246	0.242	0.250	0.160	0.153	0.156	0.145	0.171	0.272	0.262	0.220	0.193	0.154	
		Err.	8.54%	2.08%	0.08%	4.98%	7.47%	8.70%	8.94%	4.70%	3.59%	2.12%	4.93%	1.09%	0.84%	8.37%	0.43%	

It can be easily found in Fig. 9 that the maximum shape coefficients of the front faces of the double tower building is 0.77, which is close to the value of 0.8 stipulated in the Chinese code (2002). However, greater discrepancies have been noticed for the shape coefficients of back and side faces in comparison to the Chinese wind code (2002). The maximum shape coefficients of -1.25 and -0.83 for the side and back faces, respectively, were higher than the values of the Chinese code (i.e., -0.7 and -0.5, respectively). It can be deduced that noticeable differences of pressure distribution on building faces exist relative to an isolated building, for which no interaction and obstruction effect exists.

An interaction and obstruction effect exists between the main and sub-main towers, causing a change of the pressure distribution on building faces. A shielding effect is generated when one of the towers is located in front of the other tower, such as for the 180° wind direction (when the main tower is located in front of the sub-main tower, as shown in Fig. 2). In this case, the front tower produces a certain shielding effect on the rear tower and then the corresponding pressure on faces of the rear tower decreases. For the 0° wind direction, for example, the interaction and obstruction factor of face I of the main tower is less than 1, especially for the lower part of the main tower, which means that the pressure on the face I become smaller relative to single building as influence of the shielding effect of the sub-main tower. For the 180° wind direction, the interaction and obstruction factor for face VII of the sub-main tower is also less than 1 because the sub-main tower lies in the wake of the main tower, as shown in Fig. 2, and then shielding occurs on the sub-main tower.

When the main and sub-main towers are perpendicular to wind direction (such as 90° and 270° wind directions), a channeling effect is generated between the main and sub-main towers, increasing the pressure on the side faces between the two towers. It can also be noticed in Fig. 8 that all of the interaction and obstruction factors are basically larger than 1.0, when channeling occurs, such as in Fig. 8(c) “I-Exp.” and Fig.8(d) “VII-Exp.”. Higher interaction and obstruction factors result from the channeling effect, significantly increasing the wind velocity between the two towers, as shown in Fig.10, and causing an increase of the pressure on the side faces. For example, the maximum interaction and obstruction factors of faces I and VII increase to 1.32 and 1.4 for the 90° and 270° wind directions, respectively, as shown in Fig. 8(c), (f).

Interaction and obstruction effects from surrounding buildings also influence the pressure distribution on the building faces. The interaction and obstruction effect of surrounding buildings to the double tower building can be summarized as three effects: a shielding effect, a channeling effect and a re-circulating effect. When surrounding buildings lie in the inflow direction, shielding is produced; this is thought to be the most significant among the disturbance effects, as shown in Fig. 8(a) (face I), 8(b) (face VII), 8(f) (face VIII). In general, shielding always decreases the pressure coefficient on the front faces of the double tower building. Channeling influences mainly the pressure coefficient on side faces and the back faces. The re-circulating effect generally only influences the pressure coefficient on the back faces. In this study, the channeling and re-circulating effects are relatively insignificant because the surrounding buildings are far away from the target double tower, and thus the influence of surrounding buildings is negligible. The interaction and obstruction factors of face IV are almost equal to 1.0 in Fig.8(a), (c). The main reason is that the distance between the surrounding buildings and the target double tower is relatively larger, and the flow around the target double tower was not disturbed by the surrounding buildings, as shown in Fig. 10. As investigated by Wang (2011), the influence of surrounding building disappears when the separation distance between the target and surrounding buildings is larger than twice the height of the adjacent buildings.

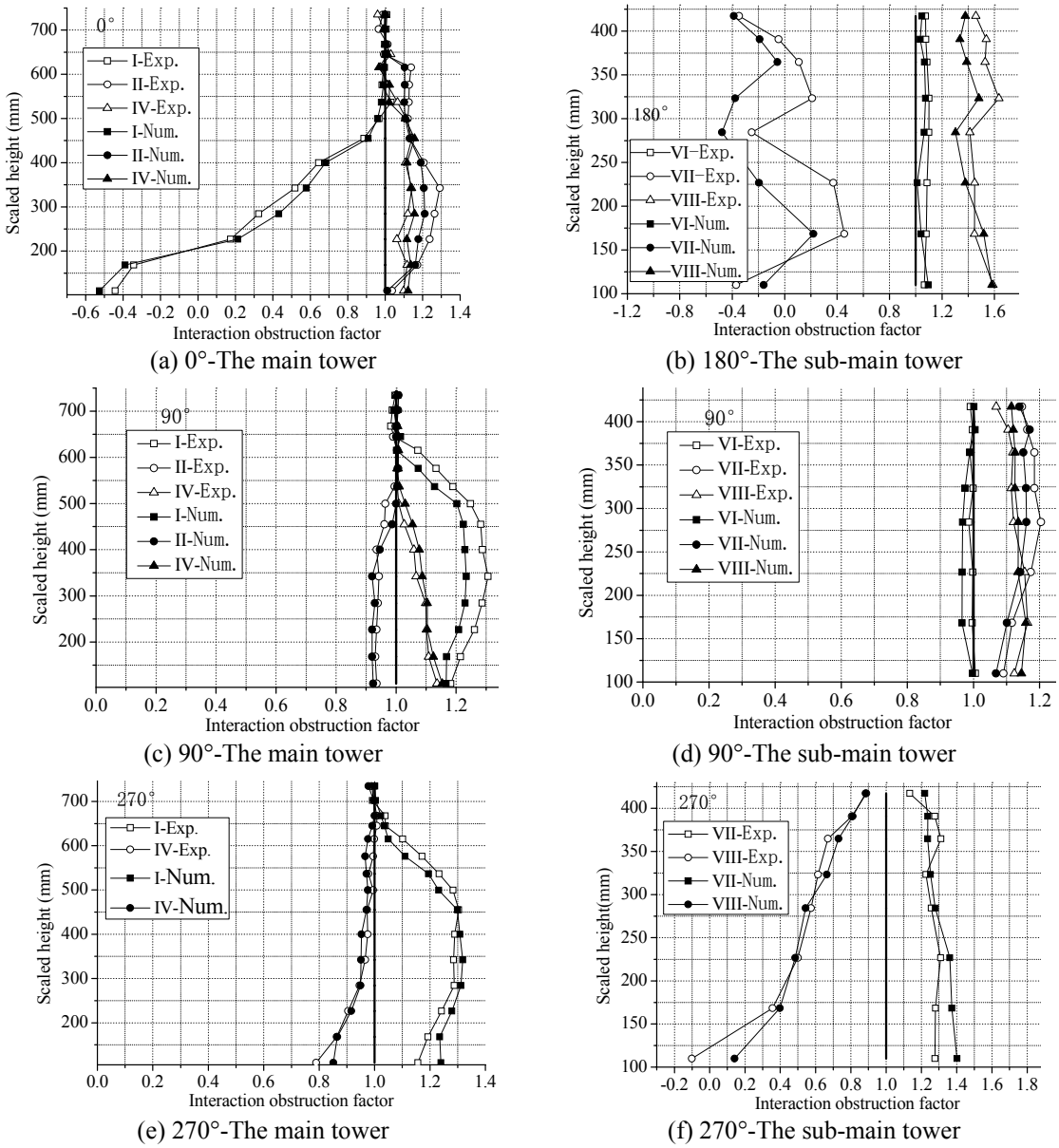

(a) 0°-The main tower (b) 180°-The sub-main tower

(c) 90°-The main tower (d) 90°-The sub-main tower

(e) 270°-The main tower (f) 270°-The sub-main tower

Fig. 8 Distribution of interaction and obstruction factor along structural height

5.4 Spatial correlation of fluctuating pressure

Spatial correlation of fluctuating wind represents statistical dependency of pressures at two taps, and is an important index of the fluctuating pressure characteristics and also spatial flow status. The lateral correlation coefficient contours of fluctuating wind pressure are shown in Fig. 11. As

revealed in the figure, the correlation coefficients decrease gradually as the distance between two pressure taps increases. The correlation coefficient is influenced by vortex structure and the surrounding flow field. The vortex shape and size and similar flow characteristics contribute to increase the correlation coefficients, given the same distance between two points. For example, the two-point correlation in the middle region is relatively larger than that of the side region of the front faces for the same spacing.

The correlation coefficients of fluctuating pressures on the side faces decrease gradually in the direction of the flow. The reason is that a sequence of vortex generation and flow separation occurs, with a similar pressure structure on the side faces. However, the vortex dimension decreases gradually, and the vortex motion become random to a certain extent, disturbing the regular flow field and resulting in a smaller correlation coefficient. It is worth mentioning that the correlation coefficients between the two side faces are not the same. Therefore it can be deduced that an asymmetric vortex state, such as vortex structure and dimension, has appeared and an asymmetric pressure distribution generated on the side faces.

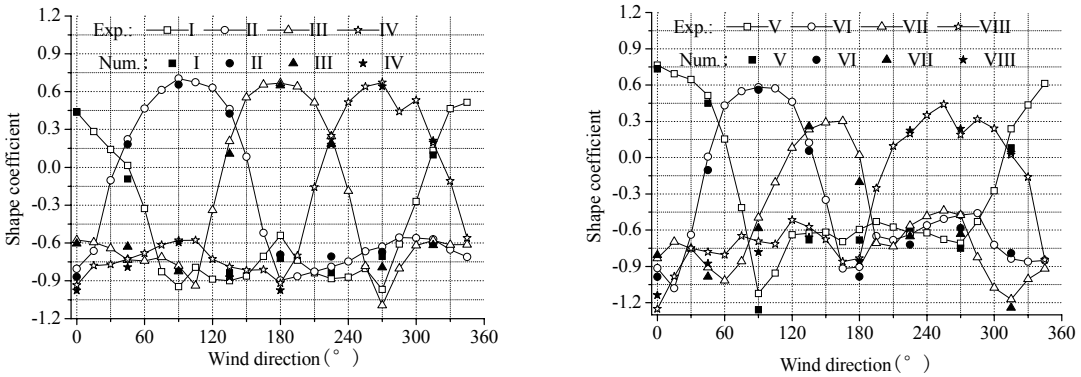

(a) The main tower (b) The sub-main tower

Fig. 9 Shape coefficients on the surfaces of the double tower buildings

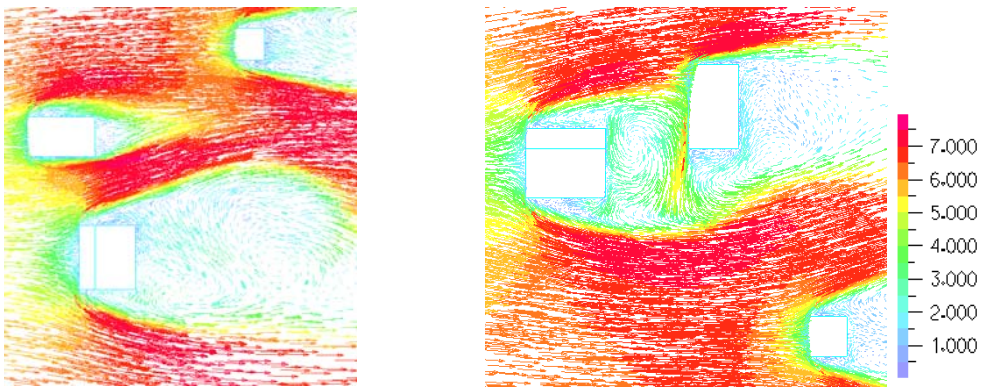

(a) 90° (b) 180°

Fig. 10 Wind velocity field at z=0.4*H* (M: Main tower, S: Sub-main tower, SU: Surrounding buildings)

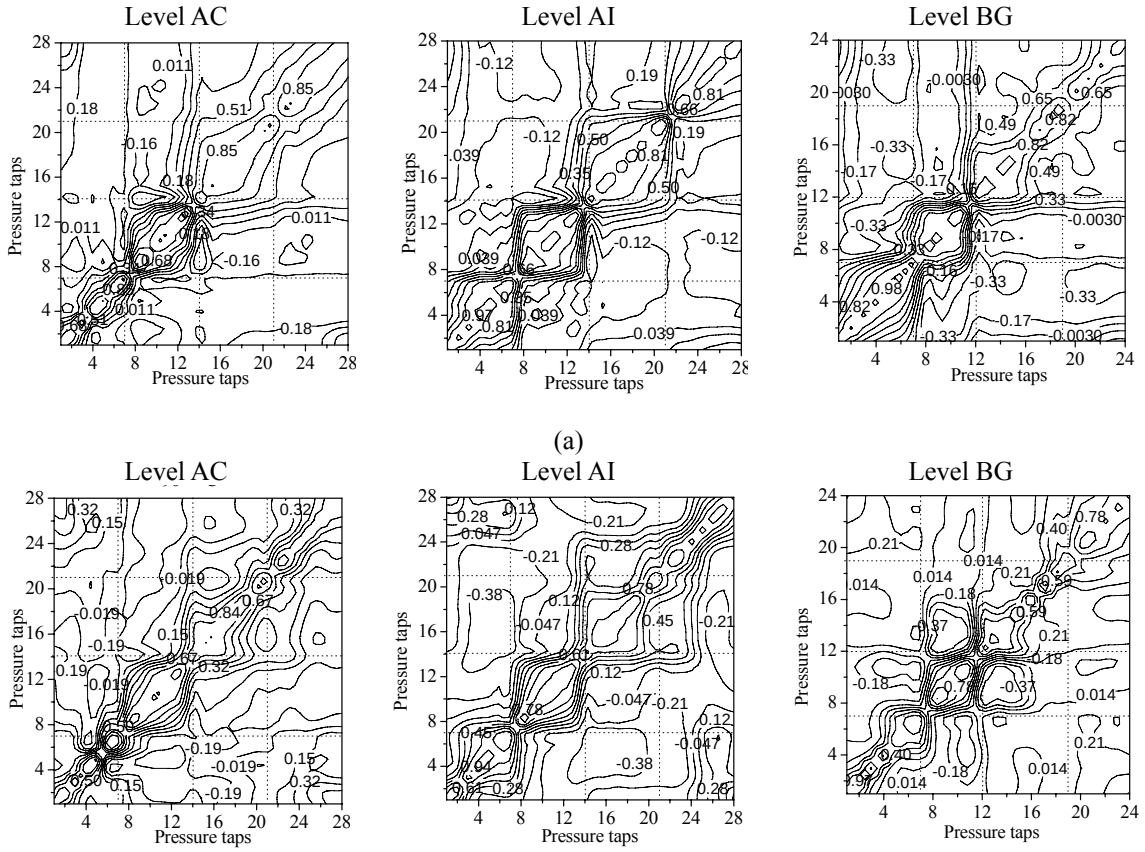

Fig. 11 Lateral correlation coefficient contours for incident wind angles: (a) 45°, and (b) 90°

The correlation coefficients of fluctuating pressures on back faces are the smallest, compared to those of front and side faces. This is because the wake flow status is disordered and irregular, differences in vortex structure and size are significant. Hence, the fluctuating pressure for taps on the back faces is incoherent, which then reduces the correlation coefficient.

The vertical correlation coefficients of fluctuating wind pressure are shown in Fig. 12, where "BB-BC (17.5 m)" denotes the vertical correlation coefficient of fluctuating pressures between level BB and BC, and the corresponding vertical distance is 17.5 m. Based on simulation results shown in the figures, the vertical correlation coefficients decrease with increasing distance between two pressure taps. When the distance between two pressure taps lies in the range of 0-30m, most of the coefficients are greater than 0.5, indicating strong correlation. When the distance is larger than 50m, the vertical correlation coefficients become smaller, implying weak correlation appears between those pressure taps.

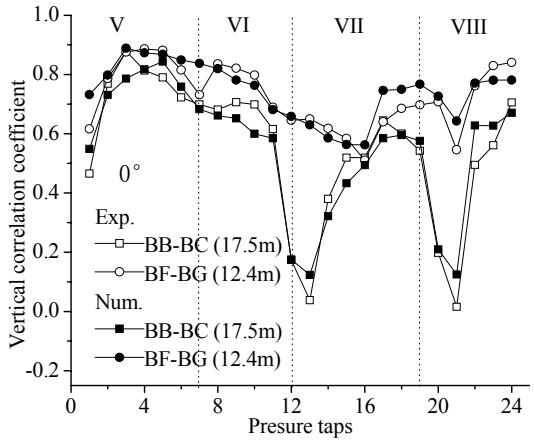

(a) 0°- The sub-main tower

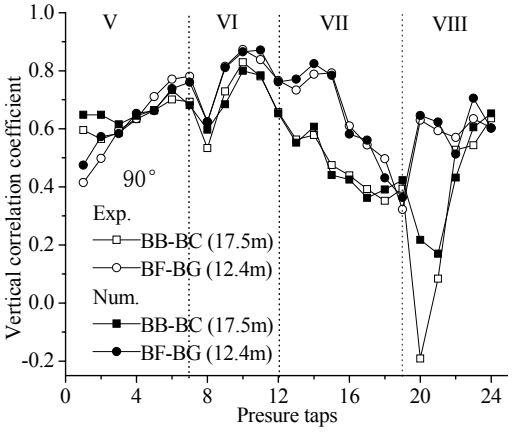

(b) 90°- The sub-main tower

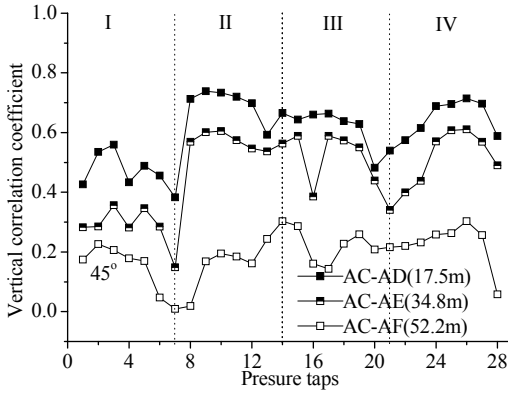

(c) 45°-The main tower (Num.)

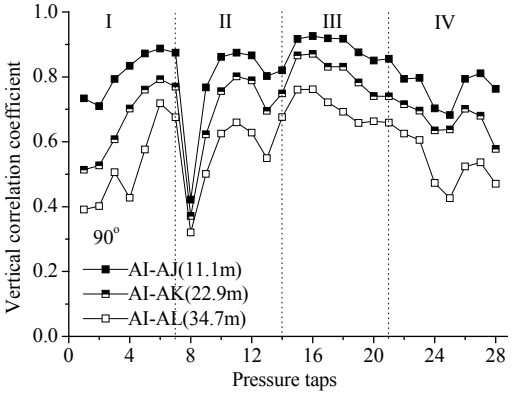

(d) 90°- The main tower (Num.)

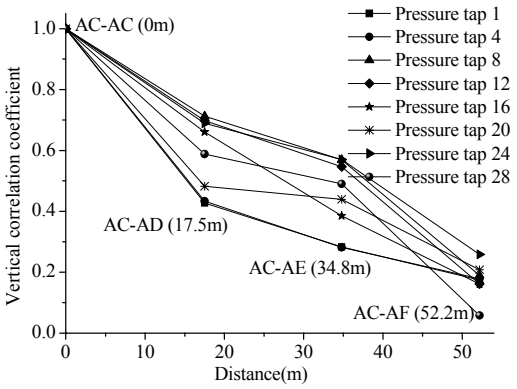

(e) 45°-The main tower (Num.)

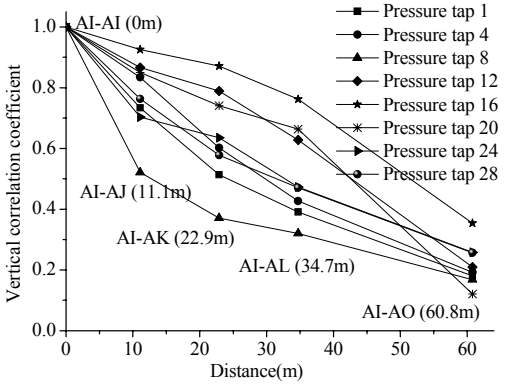

(f) 90°- The main tower (Num.)

Fig. 12 Vertical correlation coefficients for incident wind angles 0°, 45°, and 90°

6. Conclusions

A comparative study on pressure characteristics of a double tower structure has been performed using both numerical and experimental techniques. Mean and fluctuating pressure coefficients, interaction and obstruction effects, and spatial correlation have been discussed in detail, and the resulting conclusions are given as follows.

The LES method was adopted in this study, and a Smagorinsky constant of 0.1 was employed in the simulation, in view of the SGS type of model within the LES mode of the DES formulation (Breuer 2003). The length of inflow, outflow and side-flow and the total height of the computational domain were set to be large enough to avoid blockage effects from the boundary conditions. Both structured and unstructured grids were used to generate a mesh fine enough in the neighborhood of the building surfaces while keeping the mesh in far field zones from the building surfaces unchanged or in a proper coarser state. Adopting the approach proposed by Huang *et al.* (2010), the isotropic fluctuating velocity was synthesized and both mean and fluctuating wind velocity were produced on the inflow boundary, to obtain a more realistic turbulence environment. The results show that the maximum mean pressure coefficients are located on the windward surface at a height of about 0.8H-0.9H, with the minimum pressure at the corner of flow separation.

Among the 24 tested wind directions, 90º was the most unfavorable wind direction, as the maximum positive pressure and extreme negative pressure occur at this wind incident angle. The magnitude of the fluctuating pressure coefficients depend largely on the motion status of flow field. Flow with strong and orderly vortex motion yields larger fluctuating pressure, such as those on the side faces and especially at the corner of flow separation. On the contrary, irregular and random vortex motion results in smaller fluctuating pressure on the leeward faces.

The interaction and obstruction effect on the shape coefficients of the double tower building were mainly due to the interference disturbance between the main and sub-main towers, and the surrounding buildings. The interference effects of the surrounding buildings on the fluctuating pressure of the double tower building were found to be smaller than that of the main and sub-main towers. The interference is composed of three effects: a shielding effect, a channeling effect and a re-circulating effect. As discussed in this study, the shielding effect reduces the shape coefficient on the front faces greatly, especially when the main tower was upwind of the sub-main tower.

The lateral spatial correlations of fluctuating pressure on the front and side faces were relatively stronger than those on the back faces. Strong spatial correlation was found at the corner between the front and side faces. The vertical correlation decreases with increasing distance between two pressure taps. Strong vertical spatial correlations were observed for the spacing in the range of 0-30m and were substantially reduced when distance became larger than 50 m.

Acknowledgements

This project is supported by the Doctor Special Fund of Higher School (200810780001), Natural Science Foundation of Guangdong Province (8351009101000001), Production and Research Project of Ministry of Education of Guangdong Province (20090912) and Innovation Team Project of Education System of Guangzhou City (09T003). The study reported in this paper is also carried out under the support of the RGC General Research Fund, HKSAR (Project No. 9041338) and RGC Direct Allocation Grant (Project No. DAG11EG06), to which the authors

would like to express their gratitude.

References

ADINA R&D, Inc. (2005), *Theory and Modeling Guide, Volume I, II and III*, Watertown, USA.

Breuer, M., Jovičić, N. and Mazaev, K. (2003), "Comparison of DES, RANS and LES for the separated flow around a flat plate at high incidence", *Int. J. Numer. Meth. Fl.*, **41**, 357-388.

Camarri, S., Salvetti, M.V., Koobus, B. and Dervieux, A. (2002), "Large-eddy simulation of a bluff-body flow on unstructured grids", *Int. J. Numer. Meth. Fl.*, **40**, 1431-1460.

Castro, I.P. and Graham, J.G.R. (1999), "Numerical wind engineering: the way ahead?", *Proceedings of the Institution Of Civil Engineers Structures And Buildings*, **134**(3), 275-277.

Cheng, Y., Lien, F.S., Yee, E. and Sinclair, R. (2003), "A comparison of large Eddy simulations with a standard k–e Reynolds-averaged Navier–Stokes model for the prediction of a fully developed turbulent flow over a matrix of cubes", *J. Wind Eng. Ind.Aerod.s*, **91**, 1301-1328.

Clark, R., Ferziger, J. and Reynolds, W. (1979), "Evaluation of subgrid-scale models using an accurately simulated turbulent flow", *J. Fluid Mech.*, **91**, 1-16.

Cowan, I.R., Castro, I.P. and Robins A.G. (1997), "Numerical considerations for simulations of flow and dispersion around buildings", *J. Wind Eng. Ind. Aerod.*, **67-68**, 535-545.

Chinese Code (2002), *Load code for the design of building structures*, China architecture &building press, Beiiing.

Deardorff, J. (1970), "A numerical study of three-dimensional turbulent channel flow at large Reynolds numbers", *J. Fluid Mech.*, **2**, 453-480.

Fasel, H.F., Seidel, J. and Wernz, S. (2002), "A methodology for simulations of complex turbulent flows", *J. Fluid Eng.*, **4**, 933-943.

Fureby, C. (2007), "ILES and LES of complex engineering turbulent flows", *J. Fluid En.*, **12**, 1514-1524.

Guangdong Provincial Academy of Building Research (GPABR), http://www.gdjky.com/jzwl/jzfgcyjs/index.html

Gomes, M.G. and Moret, R.A. (2005), "Pedro Mendes. Experimental and numerical study of wind pressures on irregular-plan shapes", *J. Wind Eng. Ind. Aerod.*, **93**, 741-756.

Gu, M. and Huang, P. (2003), "Research history and state of art of interference effects of wind loads of a cluster of tall buildings", *J. Tongji University*, **7**, 762-766.

Hinze, J.O. (1959), *Turbulence*, McGraw-Hill: New York.

Huang, S.H., Li, Q.S. and Xu, S. L. (2007), "Numerical evaluation of wind effects on a tall steel building by CFD", *J. Constr. Steel Res.*, **63**, 612-627.

Huang, S.H., Li, Q.S. and Wu, J.R. (2010), "A general inflow turbulence generator for large eddy simulation", *J. Wind Eng. Ind. Aerod.*, **98**, 600-617.

Kose, D.A. and Dick, E. (2010), "Prediction of the pressure distribution on a cubical building with implicit LES", *J. Wind Eng. Ind. Aerod.*, **98**, 628-649.

Kraichnan, R.H. (1970), "Diffusion by a random velocity field", *Phys. Fluids*, **13**, 22-31.

Lim, H.C., Thomas, T.G. and Castro, I.P. (2009), "Flow around a cube in a turbulent boundary layer: LES and experiment", *J. Wind Eng. Ind. Aerod.*, **97**, 96-109.

Leonard, A. (1974), "Energy cascade in large-eddy simulations of turbulent fluid flows", *Adv. Geophys.*, **18**, 237-248.

Leschziner, M.A. (1993), *Computational modeling of complex turbulent flows*, In Computational Wind Engineering 1 (Ed., S. Murakami). Elsevier, Amsterdam.

Li, C., Li, Q.S. and Huang, S.H. (2007), "Large eddy simulation on wind load of a complex large-span structure", *Proceeding of the 13th Structural Wind Engineering in Chi*, Dalian, China

Murakami, S. (1998), "Overview of turbulence models applied in CWE-1997", *J. Wind Eng. Ind. Aerod.*, **74-76**, 1-24.

Murakami, S. and Mochida, A. (1995), "On turbulent vortex shedding flow past 2D square cylinder predicted by CFD", *J. Wind Eng. Ind. Aerod.*, **54**, 191-211.
Mamou, M., Tahi, A., Benmeddour, A., Cooper, K.R., Abdallah, I., Khalid, M. and Fitzsimmons, J. (2008), "Computational fluid dynamics simulations and wind tunnel measurements of unsteady wind loads on a scaled model of a very large optical telescope: A comparative study", *J. Wind Eng. Ind. Aerod.*, **96**, 257-288.
Ma, J., Chen, G.B. and Mao, Y.L. (2007), "Study of wind environment around building complex based on CFD", *J. Zhejiang University of Technol.*, **3**, 351-354.
Nozawa, K. and Tamura, T. (2002), "Large eddy simulation of the flow round a low-rise building immersed in a rough-wall turbulent boundary layer", *J. Wind Eng. Ind. Aerod.*, **90**, 1151-1162.
Obasaju, E.D. (1992), "Measurement of forces and base overturning moments on the CAARC tall building model in a simulated atmospheric boundary layer", *J. Wind Eng. Ind. Aerod.*, **40**, 103-126.
Pitsch, H. (2006), "Large-Eddy Simulation of Turbulent Combustion", *Annu. Review Fluid Mech.*, **38**, 453-482.
Rodi, W. (1997), "Comparison of LES and RANS calculation of the flowaround bluff bodies", *J. Wind Eng. Ind. Aerod.*, **69-71**, 55-75.
Shah, K.B. and Ferziger, J.H. (1997), "A fluid mechanician's view of wind engineering: large-eddy simulation of flow past a cubical obstacle", *J. Wind Eng. Ind. Aerod.*, **67**, 211-224.
Su, G. and Chen, S.H. (2006), "Numerical of simulation of wind pressures and wind environment around complex-shaped high-rise building", *Eng. Mech.*, **8**, 144-149.
Smagorinsky, J. (1963), "General circulation experiments with the primitive equations", *Monthly Weather Review*, **3**, 99-164.
Stoll, R. and Porté-Agel, F. (2008), "Large-eddy simulation of the stable atmospheric boundary layer using dynamic models with different averaging schemes", *Bound-Lay.Meterol.*, **1**, 1-28.
Sarkar, S. and Sarkar, S. (2009), "Large-Eddy Simulation of Wake and Boundary Layer Interactions Behind a Circular Cylinder", *J. Fluid. Eng.*, **9**, 091201-14
Sun, Y., Wu, Y., Lin, Z.X. and Shen, S.Z. (2007), "Non-Gaussian features of fluctuating wind pressures on long span roofs", *China Civil Engineering J.*, **4**, l-5.
Tamura, T., Okuno, A. and Sugio, Y. (2007), "LES analysis of turbulent boundary layer over 3D steep hill covered with vegetation", *J. Wind Eng. Ind. Aerod.*, **95**, 1463-1475.
Tominaga, Y., Mochida, A., Murakami, S. and Sawaki, S. (2008), "Comparison of various revised k–e models and LES applied to flow around a high-rise building model with 1:1:2 shape placed within the surface boundary layer", *J. Wind Eng. Ind. Aerod.*, **96**, 389-411.
Wang, H., Chen, S.H. and Tang, J.C. (2003), "Numerical simulation of wind pressures on a low-rise building complex with gable roofs", *Eng. Mech.*, **6**, 135-140.
Wagner, C., Hüttl, T. and Sagaut, P. (2007), *Large-Eddy Simulation for Acoustics*, Cambridge University Press.
Wang, D.Y. (2011), *Performance-Based Wind Design Method and Wind-Induced Vibration Control of High-Rise Building*, Guangzhou University: Ph.D thesis, Guangzhou, China.
Zhou, Y., Wang, D.Y. and Li Q.X. (2011), "Numerical and experimental study on wind characteristics of tall structure disturbed by surrounding buildings", *Proceedings of the 13th International Conference on Wind Engineering, Amsterdam, the Netherlands*, July.
Zhang, X.D. (2002), *Modern signal processing (the second edition)*, Beijing: Tsinghua University Press.